


## ORIGINAL ARTICLE

# A Quantitative Study on the Distribution of Mitochondria in the Neuropil of the Juvenile Rat Somatosensory Cortex

A. Santuy<sup>1</sup>, M. Turégano-López<sup>1</sup>, J.R. Rodríguez<sup>1,2</sup>, L. Alonso-Nanclares<sup>1,2</sup>, J. DeFelipe<sup>1,2</sup> and A. Merchán-Pérez <sup>1,3</sup>

<sup>1</sup>Laboratorio Cajal de Circuitos Corticales, Centro de Tecnología Biomédica, Universidad Politécnica de Madrid, Pozuelo de Alarcón, 28223 Madrid, Spain, <sup>2</sup>Departamento de Neurobiología Funcional y de Sistemas, Instituto Cajal, Consejo Superior de Investigaciones Científicas, 28002 Madrid, Spain and <sup>3</sup>Departamento de Arquitectura y Tecnología de Sistemas Informáticos, Universidad Politécnica de Madrid, Boadilla del Monte, 28660 Madrid, Spain

Address correspondence to email: [amerchan@fi.upm.es](mailto:amerchan@fi.upm.es)  [orcid.org/0000-0002-7228-5821](https://orcid.org/0000-0002-7228-5821)

## Abstract

Mitochondria play a key role in energy production and calcium buffering, among many other functions. They provide most of the energy required by neurons, and they are transported along axons and dendrites to the regions of higher energy demands. We have used focused ion beam milling and scanning electron microscopy (FIB/SEM) to obtain stacks of serial sections from the somatosensory cortex of the juvenile rat. We have estimated the volume fraction occupied by mitochondria and their distribution between dendritic, axonal, and nonsynaptic processes. The volume fraction of mitochondria increased from layer I (4.59%) to reach its maximum in layer IV (7.74%) and decreased to its minimum in layer VI (4.03%). On average, 44% of mitochondrial volume was located in dendrites, 15% in axons and 41% in nonsynaptic elements. Given that dendrites, axons, and nonsynaptic elements occupied 38%, 23%, and 39% of the neuropil, respectively, it can be concluded that dendrites are proportionally richer in mitochondria with respect to axons, supporting the notion that most energy consumption takes place at the postsynaptic side. We also found a positive correlation between the volume fraction of mitochondria located in neuronal processes and the density of synapses.

**Key words:** electron microscopy, FIB/SEM, neocortex, synapses, ultrastructure

## Introduction

The role mitochondria play in cells is vital for maintaining the function of the nervous system. They are involved in many cell processes including energy production, calcium buffering, cell differentiation, cell cycle and growth, as well as aging and death (Rizzuto et al. 2012; Tao et al. 2014; Todorova and Blokland 2017). As energy factories, they generate most of the

energy required by neurons, which is mainly used in synaptic transmission (Attwell and Laughlin 2001; Harris et al. 2012). Mitochondria are dynamic organelles that constantly undergo fission and fusion (Sakata and Jones 2003; Chen and Chan 2005; Dubinsky 2009) and they are transported up and down the axons and dendrites to those regions of the cell that require energy supply (Chang et al. 2006; Cai and Sheng 2009; MacAskill

© The Author(s) 2018. Published by Oxford University Press.

This is an Open Access article distributed under the terms of the Creative Commons Attribution Non-Commercial License (<http://creativecommons.org/licenses/by-nc/4.0/>), which permits non-commercial re-use, distribution, and reproduction in any medium, provided the original work is properly cited. For commercial re-use, please contact [journals.permissions@oup.com](mailto:journals.permissions@oup.com)

and Kittler 2010; Obashi and Okabe 2013; Schwarz 2013; Takihara et al. 2015; Devine and Kittler 2018).

Mitochondria are found closely associated with synapses and it has been shown that they can be tethered to vesicle release sites (Rowland et al. 2000), where they not only provide ATP but also act as calcium buffers (Attwell and Laughlin 2001; Li et al. 2004; MacAskill et al. 2010). Synaptic overactivity seems to recruit mitochondria to synapses, whereas prolonged synaptic silence releases mitochondria from these sites (Li et al. 2004; Obashi and Okabe 2013). In the cerebral cortex, most cortical synapses (90–98%) are established in the neuropil, which is composed of axons, dendrites, and glial processes (Alonso-Nanclares et al. 2008). Based on morphological criteria, 2 main types of synapses can be identified by electron microscopy—asymmetric and symmetric synapses (Gray 1959; Colonnier 1968; Peters and Palay 1996). Asymmetric synapses (AS) have a thickened postsynaptic density (PSD) and are in general excitatory (glutamatergic), while symmetric synapses (SS) have a thin PSD and are inhibitory (GABAergic) (Houser et al. 1984; Ascoli et al. 2008).

Previous studies on the distribution of mitochondria have been performed with techniques such as fluorescence microscopy (Chang et al. 2006; Takihara et al. 2015) and transmission electron microscopy, including the study of serial sections (Revishchin and Garey 1996; Sakata and Jones 2003; Roberts et al. 2008, 2015). An important advantage of electron microscopy is that other structures such as synapses can be identified and quantified together with mitochondria, so the possible reciprocal relationships can be established. However, obtaining long series of ultrathin sections is extremely time-consuming and difficult, often making it impossible to reconstruct large volumes of tissue. Therefore, these studies are limited by the sample size. Here we use a dual-beam electron microscope that combines a focused ion beam (FIB) and a scanning electron microscope (SEM). Using the FIB, the surface of the tissue sample is milled to a predefined depth (20 nm in our case). Then, the SEM is used to acquire an image from the freshly exposed surface. Combining both beams sequentially, we obtain long series of images automatically. These series of images, after having been piled up and aligned, represent 3D samples of tissue that can be visualized and analyzed with dedicated software. Moreover, stereological techniques can also be applied to a large number of images, thus obtaining highly reliable results. Since synapses can also be identified within these stacks, their densities and locations can also be quantified (Merchán-Pérez et al. 2014; Santuy et al. 2018b).

In previous studies on the juvenile rat somatosensory cortex we provided information on the spatial distribution of synapses in the neuropil (Anton-Sanchez et al. 2014; Merchán-Pérez et al. 2014); on the density of synapses across cortical layers and their location in dendritic shafts and spines (Santuy et al. 2018b); and on the size and shape of synaptic junctions (Santuy et al. 2018a). Given that we found significant differences in the density of synapses between cortical layers, the main goals of the present study are 1) to describe the distribution of mitochondria in the neuropil of the 6 layers of the juvenile rat somatosensory cortex; 2) to identify their location within dendrites, axons (excitatory and inhibitory) and nonsynaptic elements; and 3) to study the possible relation between the distribution of mitochondria and other tissue components such as cell somata, blood vessels and synapses. We selected this experimental animal and age to integrate these data with other anatomical, molecular, and physiological data that have already been collected from the same cortical region. The final

goal is to obtain accurate quantitative data to help understand cortical structure and to create detailed, biologically accurate models of circuitry of the primary somatosensory cortex, within the framework of the Blue Brain Project (Markram et al. 2015).

## Materials and Methods

### Tissue Preparation

Eleven Wistar rats were used for this study. They were sacrificed on postnatal day 14, by a lethal intraperitoneal injection of sodium pentobarbital (40 mg/kg) prior to intracardial perfusion of fixative. Animals to be studied by light microscopy ( $n = 8$ ) were perfused with 4% paraformaldehyde in 0.1 M phosphate buffer. Animals to be examined by electron microscopy ( $n = 3$ ) were perfused with 2% paraformaldehyde and 2.5% glutaraldehyde in 0.1 M phosphate buffer. The brain was extracted from the skull and processed for light or electron microscopy following the protocols described below.

All animals were handled in accordance with the guidelines for animal research set out in the European Community Directive 2010/63/EU, and all procedures were approved by the local ethics committee of the Spanish National Research Council (CSIC).

### Estimation of the Volume Fraction of Neuropil, Cell Somata and Blood Vessels at the Light Microscopic Level

Eight of the animals (P14–2 to P14–9) were used for this purpose. After postfixation in 4% paraformaldehyde in 0.1 M phosphate buffer, for 24 h at 4 °C, vibratome sections (100  $\mu\text{m}$  thick) were obtained from the brain. Sections containing the primary somatosensory cortex (hindlimb representation) were selected with the help of an atlas (Paxinos and Watson 2007) and flat embedded in Araldite as previously described (DeFelipe and Fairen 1993). The sections embedded in Araldite were glued on blank Araldite blocks and trimmed. Semithin sections (2  $\mu\text{m}$  thick) were obtained and stained with 1% toluidine blue in 1% borax.

Six semithin sections per animal were examined and analyzed using the Stereo Investigator integrated stereological package (Version 8.0, MicroBrightField Inc., VT, USA), attached to an Olympus BX51 light microscope (Olympus, Bellerup, Denmark), as previously described (Alonso-Nanclares et al. 2008). Four to six estimations per cortical layer were performed for each animal. Briefly, a grid of  $4 \times 4 \mu\text{m}^2$  was overlaid on the images of the semithin sections at  $\times 40$  magnification. The volume fraction occupied by the neuropil, cell somata and blood vessels was estimated by applying the Cavalieri's principle, which states that the ratio between grid points hitting the object of interest and points hitting the reference area is proportional to the volume fraction occupied by the object (Gundersen et al. 1988; Tang et al. 1997). Therefore, points hitting the neuropil, cell somata and blood vessels were independently counted in the same reference area (Fig. 1A). The volume fraction occupied by cell somata was further subdivided into neuronal and glial cell somata. Neuronal somata showed a large, lightly stained nucleus and a prominent nucleolus. Smaller neuronal somata were distinguished from astrocytes because neuronal somata show a band of clear cytoplasm around the nucleus, while astrocytes have an irregularly shaped nucleus and no apparent cytoplasm. Other glial cells

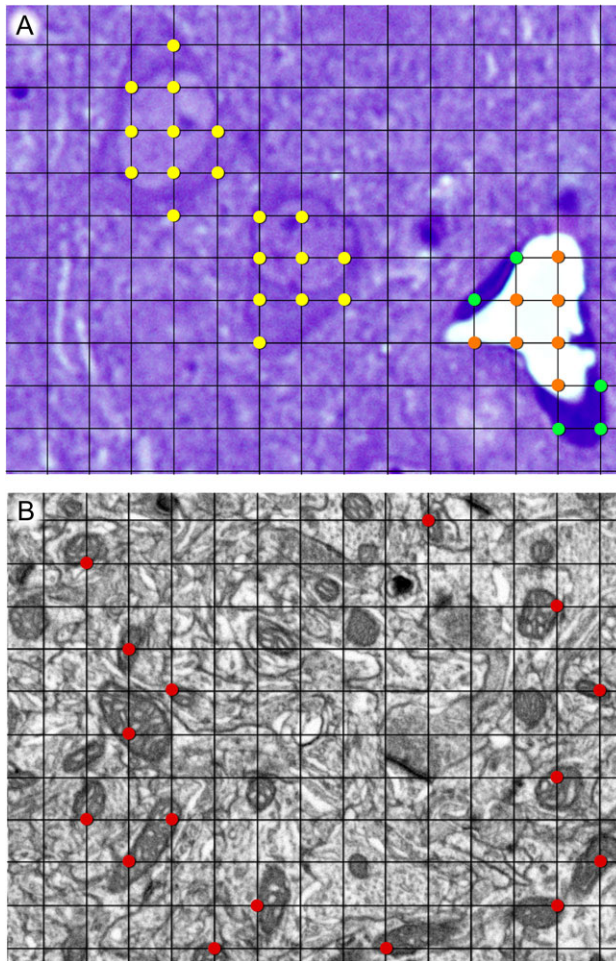


**Figure 1.** Stereological grids used for the estimation of the volume fraction of different compartments at the light (A) and electron microscopic (B) levels, using the Cavalieri method. (A) Example of the estimation of the volume fraction of neuropil, cell somata, and blood vessels at the light microscopic level. Points hitting cell somata, blood vessel lumen, and blood vessel endothelium have been highlighted in yellow, orange, and green, respectively. The remaining points hit the neuropil, although they have not been highlighted for the sake of clarity. (B) Example of one stereological grid used for the estimation of the volume fraction of mitochondria at the electron microscopic level. Points hitting mitochondria have been highlighted in red. The ratio of grid points hitting any compartment to points hitting the reference area is proportional to the volume fraction occupied by that compartment (see Materials and Methods for details). The thickness of grid lines and the size of marked points have been exaggerated for clarity. Grid size is  $4 \times 4 \mu\text{m}^2$  in (A) and  $500 \times 500 \text{nm}^2$  in (B).

(microglia and oligodendrocytes) have darkly stained nuclei (García-Cabezas et al. 2016). The volume fraction of blood vessels was also subdivided into the volume fraction of endothelial cells and vessel lumen. The volume fraction occupied by all these compartments was estimated in layers I–VI.

### Estimation of the Volume Fraction of Axons, Dendrites, Nonsynaptic Elements and Mitochondria at the Electron Microscopic Level

Three animals (w31, w33, and w35) were processed for focused ion beam milling and scanning electron microscopy (FIB/SEM), according to a previously described protocol (Merchán-Pérez et al. 2009; Santuy et al. 2018a, 2018b). Animals were administered an intraperitoneal injection of sodium pentobarbital

(40 mg/kg) and were intracardially perfused with 2% paraformaldehyde and 2.5% glutaraldehyde in 0.1 M phosphate buffer (PB). The brains were extracted from the skull and postfixed at 4 °C overnight in the same solution. Vibratome sections were obtained (150  $\mu\text{m}$  thick) and they were osmicated for 1 h at room temperature in PB with 1% OsO<sub>4</sub>, 7% glucose, and 0.02 M CaCl<sub>2</sub>. After washing in PB, the sections were stained en bloc for 30 min with 1% uranyl acetate in 50% ethanol at 37 °C, and were then flat-embedded in Araldite.

A Crossbeam® Neon40 EsB electron microscope was used (Carl Zeiss NTS GmbH, Oberkochen, Germany). This instrument combines a gallium FIB and a high-resolution field emission SEM column. The gallium FIB was used to mill the sample surface, removing thin layers of material (20 nm thick) in each cycle. After removing each layer, the milling process was paused, and the freshly exposed surface was imaged at 1.8 kV acceleration potential using the in-column backscattered electron detector. The milling and imaging processes were sequentially repeated, and long series of images were acquired through a fully automated procedure, thus obtaining a stack of images that represented a 3D sample of the tissue (Merchán-Pérez et al. 2009). In total, 29 different stacks of the neuropil were obtained from the 6 layers of the somatosensory cortex (3 samples from layer I, 4 from layer II, 10 from layer III, 5 from layer IV, 3 from layer V, and 4 from layer VI). Image resolution in the xy plane ranged from 3.7 to 4.5 nm/pixel (equivalent magnification of  $\times 15\,000$  and  $\times 12\,410$ , respectively). Resolution in the z axis (equivalent to section thickness) was 20 nm. We obtained images of  $2048 \times 1536$  pixels, so the field of view was  $7.56 \times 5.68 \mu\text{m}^2$  at 3.7 nm/pixel. Line averaging was used for noise reduction, and the acquisition time per image was approximately 4 min. Although better resolutions can be obtained with FIB/SEM, we chose these parameters as a compromise solution to obtain a large enough field, in a period of time that allowed us to acquire between 189 and 363 serial sections per stack (mean: 254.66; total: 7385 sections).

For the estimation of the volume fraction of dendrites, axons, and nonsynaptic elements that compose the neuropil, we used the Image J Stereology Toolset (Mironov 2017) to analyze 13 of the stacks of images described above (Fig. 1B). A grid with an area per point of  $400\,000 \text{nm}^2$  was used. The estimations were made in every 40th section of each stack ( $z = 800 \text{nm}$ ). A total of 64 sections were analyzed (11 from layer I, 8 from layer II, 15 from layer III, 9 from layer IV, 10 from layer V, and 11 from layer VI). To identify the different components of the neuropil, the stack of images was navigated in 3D with the help of EspINA software (Morales et al. 2011). The cell processes that were hit by a point of the stereological grid were followed through the stack until it was determined whether they established synapses or not. Grid points hitting fibers that were postsynaptic with respect to at least one synaptic junction were classified as “dendritic,” and when they were presynaptic to at least one synaptic junction, they were classified as “axonic”. Axons were further classified as excitatory axons if they established AS, or as inhibitory axons if the synapses that they established were SS. Points hitting myelinated fibers were classified as “myelinated axons.” Other cell processes not showing any synaptic contact within the stack were tagged as “nonsynaptic.” These nonsynaptic elements include glial processes, as well as axons and dendrites that do not establish synapses within the volume of the stack of images. The volume fraction of mitochondria was estimated in the 29 stacks of images using the same Image J Stereology Toolset described above (Mironov 2017). The area per point selected for the grid was  $250\,000 \text{nm}^2$ ,

and counting was carried out in every 10th section of each stack ( $z = 200$  nm). A total of 752 sections were analyzed (79 from layer I, 94 from layer II, 253 from layer III, 122 from layer IV, 92 from layer V, and 112 from layer VI). Identification of the cellular compartment where mitochondria were located (“dendritic,” “axonic,” or “nonsynaptic”) was carried out using the same criteria described above. In all stereological studies, the parameters used for the Cavalieri method (grid size and number of sections) were chosen based on pilot studies for each of the analyses that have been performed (Broskey et al. 2013). Coefficients of error and variation were calculated to ensure the reliability of the measurements (Howard and Reed 2005) (Supplementary Tables S1–S3).

To select the exact location of the samples, we first obtained plastic semithin sections ( $2\ \mu\text{m}$  thick) from the block surface and stained them with toluidine blue to identify cortical layers. These sections were then photographed with a light microscope. The last of these light microscope images (corresponding to the section immediately adjacent to the block face) was then collated with SEM photographs of the surface of the block. In this way, it was possible to accurately identify the regions of the neuropil to be studied (Fig. 2, Supplementary Video 1). These samples have previously been used to study the distribution and size of synapses (Anton-Sanchez et al. 2014; Merchán-Pérez et al. 2014; Santuy et al. 2018a, 2018b). Synaptic junctions within these volumes were visualized, automatically segmented, and reconstructed in 3D with EspINA software (Morales et al. 2011). Synapses were identified according to well-established criteria (Peters et al. 1991; Peters and Palay 1996), when the following elements were clearly recognized: synaptic vesicles in the presynaptic side and electron-dense

thickenings on the cytoplasmic faces of the pre and postsynaptic membranes. Synaptic junctions with either a prominent or thin PSD were classified as asymmetric or symmetric synaptic junctions, respectively (Merchán-Pérez et al. 2009).

## Statistics

Normality and homoscedasticity were analyzed with the Shapiro–Wilk and Levene tests, respectively. When the data were parametric (normality and homoscedasticity criteria were met), we performed ANOVA test, followed by Bonferroni test for pair-wise comparisons. When the necessary assumptions for ANOVA were not satisfied, we used the Kruskal–Wallis test (KW), followed by the Mann–Whitney test (MW) for pair-wise comparisons. Chi-square tests were used for contingency tables, and linear regression was used to find correlations. Analyses were performed with SPSS software (IBM Corp. Released 2013. IBM SPSS Statistics for Windows, Version 22.0. Armonk, NY: IBM Corp) and GraphPad (GraphPad Prism version 5.00 for Windows, GraphPad Software, San Diego, CA, USA).

## Results

### Volume Fraction of Neuropil, Cell Somata, and Blood Vessels

The volume fraction of cortex occupied by neuropil, cell somata, and blood vessels was estimated in the 6 layers of the cortex (Table 1 and Fig. 3). The neuropil was the major component of the cortex, especially in layer I, where it reached a mean value of 93.23%, clearly larger than any of the other layers (MW test,  $P < 0.0001$ ). The mean volume fraction of

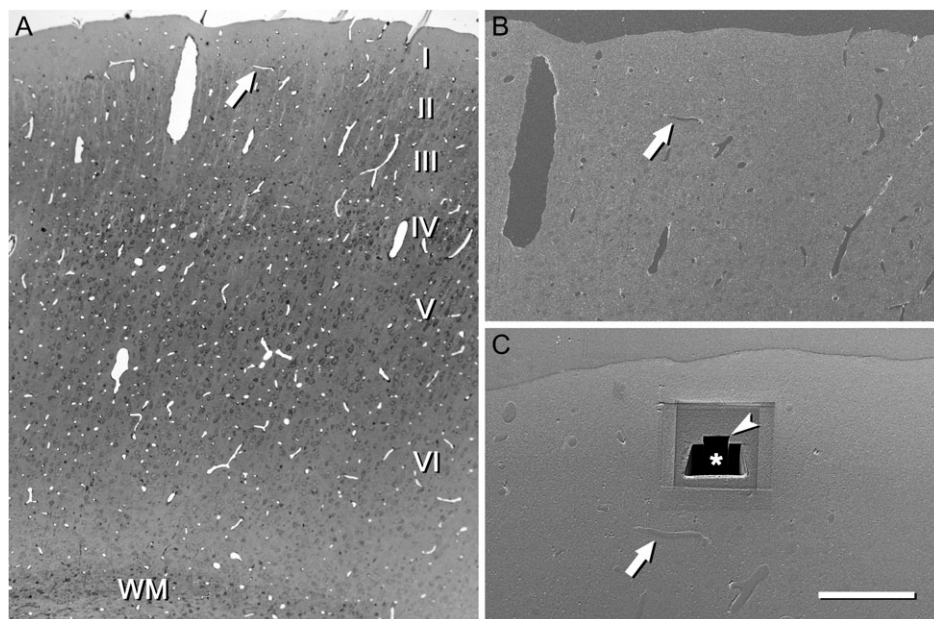


**Figure 2.** An example of the use of a semithin section to locate the region of interest. (A) Semithin section of the somatosensory cortex stained with toluidine blue and photographed with an optical microscope. This section is immediately adjacent to the block face that was later photographed with the SEM. Cortical layers (I–VI) and white matter (WM) can be identified. Blood vessel profiles can be used as reference points to locate the region of interest. In this particular example, a vascular profile (arrow) is located approximately in the boundary between layers I and II. (B) Low power electron micrograph acquired with the SEM from the block surface. The same vascular profile that was previously identified in the semithin section is also visible on the block face (arrow). (C) The same block after a series of images has been acquired with the FIB/SEM. The reference blood vessel (arrow) was used to locate layer I. First, a large trench (asterisk) was excavated with the FIB in order to have visual access to the tissue below the block surface. Then, a smaller trench (arrow head) was sequentially milled with the FIB and photographed with the SEM at intervals of 20 nm, thus obtaining a series of images. A similar procedure was used to locate the regions of interest in all other cortical layers. Scale bar = 300, 150, and  $80\ \mu\text{m}$  in (A), (B), and (C), respectively. See also Supplementary Video 1.

**Table 1** Volume fraction (percentage  $\pm$  standard error of the mean [sem]) of neuropil, cell somata, and blood vessels, in the 6 layers of the cortex, and averaged for all layers (I–VI). The volume fraction of cell somata has been subdivided into the volume fraction of neuronal and glial somata. The volume fraction of blood vessels has also been subdivided into the volume fraction of the lumen and endothelium

Volume fraction of neuropil, cell somata, and blood vessels (% $\pm$ sem)					
Layer	Neuropil	Neuronal somata	Glial somata	Blood vessel lumen	Endothelium
I	93.23 $\pm$ 2.34	2.23 $\pm$ 1.57	1.30 $\pm$ 0.61	2.33 $\pm$ 0.91	0.91 $\pm$ 0.70
II	77.39 $\pm$ 3.84	16.10 $\pm$ 2.86	2.38 $\pm$ 1.01	2.66 $\pm$ 0.83	1.48 $\pm$ 0.56
III	80.12 $\pm$ 2.72	13.06 $\pm$ 2.02	1.83 $\pm$ 0.36	3.89 $\pm$ 1.78	1.10 $\pm$ 0.68
IV	78.10 $\pm$ 3.15	15.99 $\pm$ 2.25	2.36 $\pm$ 0.86	2.61 $\pm$ 1.15	0.95 $\pm$ 0.49
V	80.52 $\pm$ 1.60	13.55 $\pm$ 1.49	2.45 $\pm$ 0.54	2.68 $\pm$ 1.52	0.80 $\pm$ 0.15
VI	79.10 $\pm$ 3.18	15.68 $\pm$ 2.97	2.01 $\pm$ 0.83	2.53 $\pm$ 0.92	0.68 $\pm$ 0.37
I–VI	81.28 $\pm$ 5.41	12.88 $\pm$ 4.87	2.11 $\pm$ 4.59	2.77 $\pm$ 0.52	0.96 $\pm$ 2.64

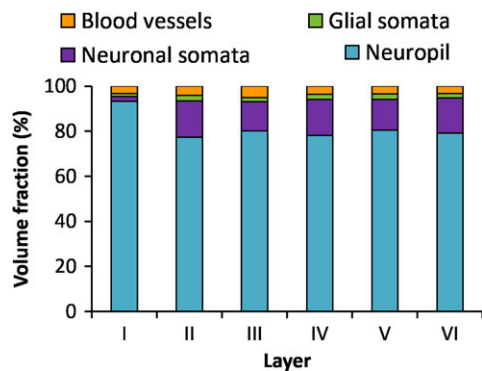


**Figure 3.** Volume fraction of neuropil, cell somata, and blood vessels in the 6 layers of the cortex. Volume fraction of neuropil (blue), neuronal somata (purple), glial somata (green), blood vessels (lumen and endothelium, orange) in the 6 layers of the cortex.

neuropil was similar in layers II–VI, ranging from 77.39% in layer II to 80.86% in layer VI, with no statistically significant differences (KW test,  $P = 0.34$ ) (Table 1 and Fig. 3). The volume fraction of cell somata, comprising neuronal and glial somata, was the smallest in layer I (3.53%, Table 1) and this difference was statistically significant when compared with any of the other layers (MW tests  $P < 0.0001$ ), where it ranged from 15.42% in layer III to 18.48% in layer II. If we consider the volume fraction of neuronal somata alone, the difference between layer I (2.23%) and any of the remaining layers (13.06–16.10%) was also statistically significant (MW tests,  $P < 0.0001$ ), while differences between layers II and VI were not. The volume fraction of neuronal somata was larger than the volume fraction of glial somata in all layers except layer I (MW tests,  $P = 0.16$  in layer I,  $P < 0.0001$  in layers II–VI). Finally the smallest volume fraction was occupied by blood vessels in all layers, ranging from 3.33% in layer V to 4.99% in layer III, with no statistically significant differences between layers (ANOVA  $P = 0.061$ ).

### Volume Fraction of Dendrites, Axons, and Nonsynaptic Elements in the Neuropil

To further analyze the composition of the neuropil, we estimated the volume fraction of dendrites, axons, and nonsynaptic elements at the electron microscopic level (Table 2 and Fig. 4, Supplementary Video 1).

The volume fraction of neuropil occupied by dendrites decreased from layer I (46.31%) to layer VI (26.03%), although no statistical differences between layers were found (KW,  $P = 0.07$ ) (Fig. 5 and Table 2). The volume fraction of axons was lower

than the volume fraction of dendrites in all layers, ranging from 19.75% in layer I to 26.19% in layer II (Fig. 5 and Table 2). Excitatory axons (those establishing AS, see Materials and Methods) were clearly predominant over inhibitory axons (those establishing SS). The mean volume fractions of excitatory and inhibitory axons were 18.78% and 3.01%, respectively (t test,  $P < 0.0001$ ) (Fig. 6 and Table 2). The volume fraction of excitatory axons was maximal in layer II (22.64%) and minimal in layer VI (14.98%). The volume fraction of inhibitory axons varied between 3.55% in layers II and IV and 1.84% in layer VI. Differences between layers were not statistically significant for excitatory or inhibitory axons (KW tests,  $P = 0.23$  and  $P = 0.82$ , respectively). Myelinated axons were only found in layers IV–VI, with volume fractions that rose from 0.38% in layer IV to 4.63% in layer VI (Fig. 6 and Table 2). Finally, the volume fraction of nonsynaptic elements was similar in layers I–IV, ranging from 31.09% to 37.78%, and it showed a tendency to increase in layers V (39.51%) and VI (52.52%), although the differences between layers were not statistically significant (KW,  $P = 0.20$ ) (Fig. 5 and Table 2).

### Volume Fraction of Mitochondria in the Neuropil

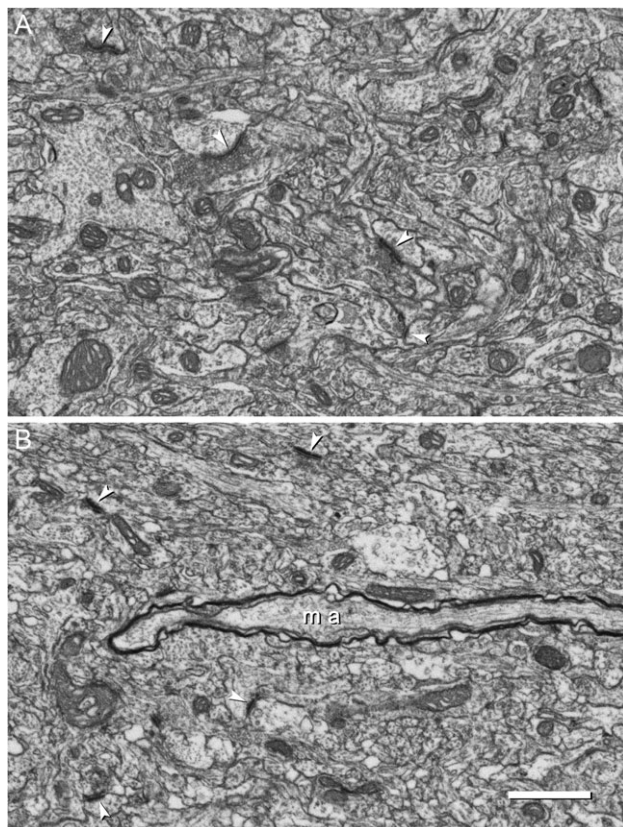
We studied the volume fraction of neuropil occupied by mitochondria, as well as the proportions of mitochondria that were located in different subcellular compartments (dendrites, axons, and nonsynaptic elements). The volume fraction of mitochondria increased from layer I (4.59%) to reach its maximum in layer IV (7.74%) and decreased to its minimum in layer VI (4.03%) (Table 3 and Fig. 7). Statistically significant differences were found between layer IV and all the other layers, and between layer III and all other layers except layer V (MW,  $P < 0.036$ ).

Once we had estimated the volume fraction of mitochondria in the neuropil, we estimated the proportion of mitochondrial volume located in axons, dendrites, and nonsynaptic elements (Table 3 and Fig. 7). Most of the mitochondrial volume (58.58% on average) was located in dendrites and axons, while 41.42% was located in nonsynaptic elements. Considering only mitochondria located in axons or dendrites, we found that mitochondria located in dendrites (74.38%) clearly predominated over mitochondria located in axons (25.62%) (Table 3 and Fig. 7). In layer I, the predominance of dendritic mitochondria versus axonic mitochondria was the highest (79.43% vs. 20.57%), and this difference was statistically significant when compared with the other layers ( $\chi^2$  test,  $P = 0.025$ ).

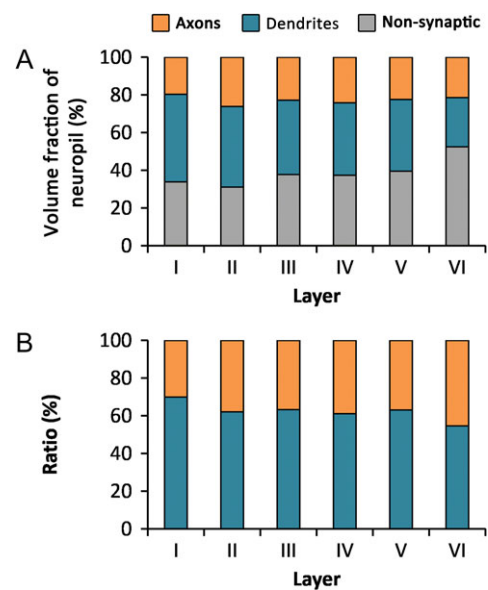
Considering only the axonal compartment, the volume fraction of mitochondria located in excitatory axons was, on average, 74.57% of all mitochondria located in axons, followed by

**Table 2** Volume fraction of dendrites, axons, and nonsynaptic elements in the neuropil. Volume fractions are indicated in percentage of neuropil occupied by dendrites, axons, and nonsynaptic elements  $\pm$  sem

Volume fraction of dendrites, axons, and nonsynaptic elements in the neuropil (% of neuropil $\pm$ sem)					
Layer	Dendrites	Excitatory axons	Inhibitory axons	Myelinated axons	Nonsynaptic elements
I	46.31 $\pm$ 2.53	16.56 $\pm$ 0.34	3.20 $\pm$ 0.16	0.00 $\pm$ 0.00	33.93 $\pm$ 2.03
II	42.72 $\pm$ 0.02	22.64 $\pm$ 1.83	3.55 $\pm$ 0.69	0.00 $\pm$ 0.00	31.09 $\pm$ 2.54
III	39.35 $\pm$ 0.19	19.72 $\pm$ 0.55	3.15 $\pm$ 0.20	0.00 $\pm$ 0.00	37.78 $\pm$ 1.14
IV	38.45 $\pm$ 2.36	20.33 $\pm$ 0.47	3.55 $\pm$ 0.49	0.38 $\pm$ 0.24	37.29 $\pm$ 2.62
V	38.16 $\pm$ 2.61	18.42 $\pm$ 0.27	2.79 $\pm$ 0.56	1.13 $\pm$ 0.92	39.50 $\pm$ 2.71
VI	26.03 $\pm$ 2.43	14.98 $\pm$ 0.64	1.84 $\pm$ 0.77	4.63 $\pm$ 0.65	52.52 $\pm$ 3.20
I–VI	38.50 $\pm$ 2.80	18.78 $\pm$ 0.91	3.01 $\pm$ 1.12	1.02 $\pm$ 0.74	38.69 $\pm$ 0.26

**Figure 4.** Electron micrographs of the neocortical neuropil obtained by FIB/SEM. These examples belong to 2 series of images that were acquired from layer III (A) and layer VI (B). Mitochondria of different sizes and shapes are scattered throughout the field of view. Synapses are also visible; some of them have been pointed by arrow heads. A myelinated axon (ma) appears in the image corresponding to layer VI. In this particular example, the myelinated axonal segment does not contain any mitochondria. Scale bar = 1  $\mu$ m. See also Supplementary Video 1.

mitochondria located in inhibitory axons (22.73%) and mitochondria located in myelinated axons (2.70%). Although there seemed to be a tendency for the proportion of mitochondria located in inhibitory axons to increase towards infragranular layers, the differences across layers were not statistically significant (KW,  $P = 0.061$ ). Mitochondria in myelinated axons were only found in layers V and VI (Table 3 and Fig. 8). Mitochondria were not detected in the very few myelinated axons of layer IV observed in our samples. The volume fraction of these axons in this layer was very low (0.38%, Table 2). Thus,

**Figure 5.** Volume fraction of axons, dendrites, and nonsynaptic elements in the neuropil. (A) Volume fraction of axons (orange), dendrites (blue), and nonsynaptic elements (gray) in the neuropil of the 6 layers of the cortex. (B) Ratio between the axonal (orange) and dendritic (blue) compartments in the neuropil.

the volume fraction of mitochondria located in myelinated axon segments of layer IV must be even lower.

As we have seen, the volume fraction of dendritic mitochondria was higher than the volume fraction of axonic mitochondria. This could simply be due to the fact that the volume fraction of dendrites is larger than the volume fraction of axons, but there is also the possibility that mitochondria preferentially accumulate in dendrites over axons. In order to analyze whether mitochondria were preferentially located in any of the subcellular compartments of the neuropil, we calculated the ratio between the volume fraction of mitochondria located in the 3 compartments of the neuropil (dendritic, axonal, or nonsynaptic) and the volume fraction of these compartments, respectively. These ratios were calculated from Tables 2 and 3 and would be equal to 1.00 if mitochondria were not preferentially located in any of the compartments (Fig. 9). The ratio for dendritic mitochondria was 1.15 on average, indicating that mitochondria are proportionally more abundant in dendrites, with the exception of layer I, where the ratio was close to 1.00 (0.94). The ratio for mitochondria located in nonsynaptic elements was 1.08 on average, although it varied between 0.88 and 1.34 in different layers. For mitochondria located in

excitatory axons, the ratio was below 1.00 in all layers, with an average of 0.59, suggesting that mitochondria are proportionally less abundant in excitatory axons than in dendrites. In the case of inhibitory axons the ratio was 1.13 on average. Inhibitory axons showed the widest variations; the ratio increased from 0.33 in layer I to much higher values in infragranular layers (up to 1.95 in layer V) (Fig. 9).

### Correlation Between Volume Fraction of Mitochondria and the Density of Synapses

The density of excitatory and inhibitory synapses in the hindlimb representation of the somatosensory cortex of the P14 rat has been previously described (Santuy et al. 2018b). That study was performed on the same stacks of serial images used here, so we can correlate the density of synapses in these stacks with their mitochondrial volume fraction. We found a positive correlation ( $R^2 = 0.49$ ) between synaptic density and mitochondrial volume fraction (Fig. 10). It is interesting to note that a similar correlation was found between synaptic density and dendritic mitochondria ( $R^2 = 0.46$ ). However, the correlation with synaptic density was lower with axonic mitochondria ( $R^2$

$= 0.30$ ) and lacking with mitochondria located in nonsynaptic elements ( $R^2 = 0.03$ ).

We found no correlations between the volume fraction of mitochondria and the volume fraction of neuropil ( $R^2 = 0.15$ ), cell somata ( $R^2 = 0.12$ ), or blood vessels ( $R^2 = 0.15$ ).

## Discussion

The present study provided 3 main findings. First, the volume fraction of mitochondria increased from layer I to reach its maximum in layer IV and decreased to its minimum in layer VI. Second, our results indicate that dendrites are proportionally richer in mitochondria with respect to axons. Third, we found a positive correlation between mitochondria located in neuronal processes and the density of synapses, while there was no correlation with mitochondria located in nonsynaptic elements.

### Volume Fraction of Neuropil, Cell Somata, and Blood Vessels

Neuropil is the main component of all layers of the somatosensory cortex, followed by neuronal somata, blood vessel lumen, glial somata and endothelium. The proportions of all these cortical components are very similar in layers II–VI. Layer I shows a clearly different pattern of organization when compared with the other cortical layers, since it has the lowest density of neuronal somata, glial somata, and blood vessels, and has the highest volume fraction of neuropil. The scarce population of cells in layer I is mainly composed by GABAergic interneurons (Muralidhar et al. 2014), while excitatory neurons are almost absent (Anderson et al. 1992). Layer I differs in other parameters such as the spatial distribution of synapses, since the distance of synapses to their nearest neighbors tends to be larger than in the other layers (Anton-Sanchez et al. 2014). In addition, the proportion of perforated and horseshoe-shaped synapses in layer I is larger than in any of the other layers (Santuy et al. 2018a). Layer I also differs in terms of the volume fraction of mitochondria (see below).

### Volume Fraction of Mitochondria

Mitochondria constantly undergo fission and fusion and their sizes are very variable (Shaw and Nunnari 2002; Brocard et al. 2003; Chen and Chan 2005; Dubinsky 2009). Therefore, for a quantitative estimation of mitochondria, counting individual mitochondrial profiles should be complemented with areal measurements of these profiles, or with stereological methods (Carroll and Wong-Riley 1984; Sumpster et al. 1986; Wong-Riley

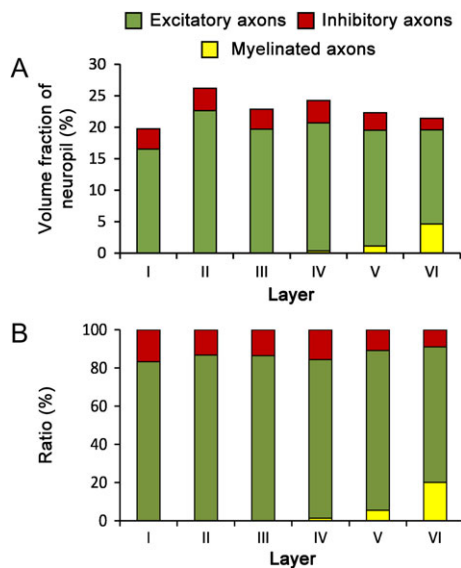


**Figure 6.** Volume fraction of excitatory and inhibitory axons. (A) Volume fraction of excitatory (green), inhibitory (red), and myelinated axons (yellow) in the neuropil of the 6 cortical layers. (B) Ratio between the volumes of excitatory, inhibitory, and myelinated axons in the neuropil of the 6 cortical layers.

**Table 3.** Volume fraction of mitochondria in the cortical neuropil. Volume fractions of mitochondria (leftmost column) are given in percentage  $\pm$  sem for the 6 cortical layers. The percentage of mitochondrial volume located in dendrites, axons, and nonsynaptic elements is also given for the 6 layers

Layer	Volume fraction of mitochondria (% $\pm$ sem)	Percentage of mitochondrial volume located in different subcellular compartments (% $\pm$ sem)				
		Dendrites	Excitatory axons	Inhibitory axons	Myelinated axons	Nonsynaptic elements
I	4.59 $\pm$ 0.04	43.44 $\pm$ 3.01	10.21 $\pm$ 2.11	1.04 $\pm$ 0.57	0.00 $\pm$ 0.00	45.31 $\pm$ 5.42
II	5.22 $\pm$ 0.31	46.50 $\pm$ 3.79	12.92 $\pm$ 1.67	2.36 $\pm$ 0.72	0.00 $\pm$ 0.00	38.22 $\pm$ 3.15
III	6.40 $\pm$ 0.22	48.70 $\pm$ 2.71	14.35 $\pm$ 1.13	3.89 $\pm$ 0.59	0.00 $\pm$ 0.00	33.06 $\pm$ 3.04
IV	7.74 $\pm$ 0.39	43.92 $\pm$ 2.56	13.53 $\pm$ 0.76	4.59 $\pm$ 0.67	0.00 $\pm$ 0.00	37.96 $\pm$ 2.40
V	5.75 $\pm$ 0.49	42.67 $\pm$ 3.20	10.04 $\pm$ 2.76	5.43 $\pm$ 1.71	0.81 $\pm$ 0.54	41.05 $\pm$ 5.40
VI	4.03 $\pm$ 0.32	36.21 $\pm$ 0.94	6.11 $\pm$ 0.94	3.16 $\pm$ 0.58	1.62 $\pm$ 0.19	52.91 $\pm$ 2.51
I-VI	5.62 $\pm$ 0.54	43.57 $\pm$ 1.73	11.19 $\pm$ 1.25	3.41 $\pm$ 0.65	0.40 $\pm$ 0.28	41.42 $\pm$ 2.82

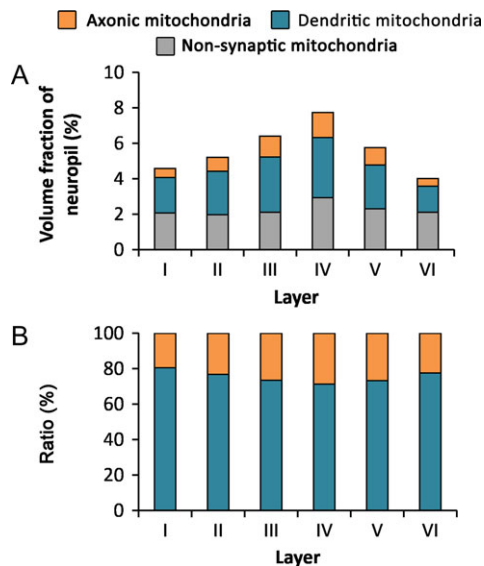


**Figure 7.** Volume fraction of mitochondria located in axons, dendrites, and non-synaptic elements in the neuropil. (A) Volume fraction of mitochondria located in axons (orange), dendrites (blue), and nonsynaptic elements (gray) in the 6 layers of the cortex. (B) Ratio between mitochondrial volume located in axonal (orange) and dendritic (blue) elements in the 6 layers of the cortex. See also Table 3.

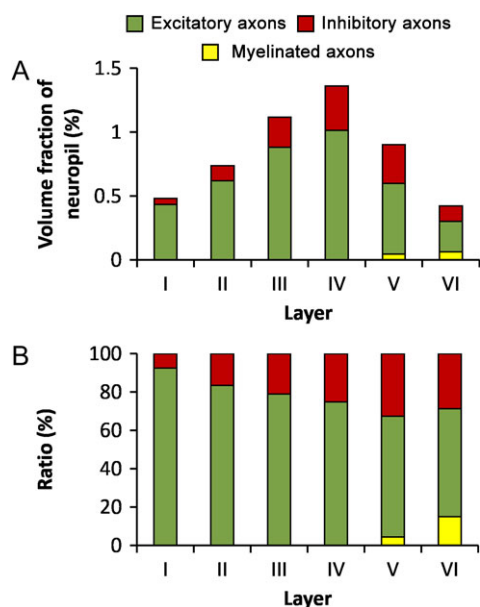


**Figure 8.** Volume fraction of mitochondria located in axons. (A) Volume fraction of mitochondria located in excitatory (green), inhibitory (red), and myelinated (yellow) axons in the 6 cortical layers. (B) Ratio between the volumes of mitochondria located in excitatory, inhibitory and myelinated axons in the neuropil of the 6 cortical layers. See also Table 3.

1989). The use of serial sections further improves the quantification of mitochondria, and their relationship with other subcellular structures—particularly synapses—can be better established (Roberts et al. 2008, 2015; Rodriguez-Moreno et al. 2017). In the present study, we have used 29 series of sections (on average, 254.66 sections per stack, 20 nm thick) that represent 3D samples of neuropil from the 6 cortical layers. Taking advantage of this, we have performed the stereological

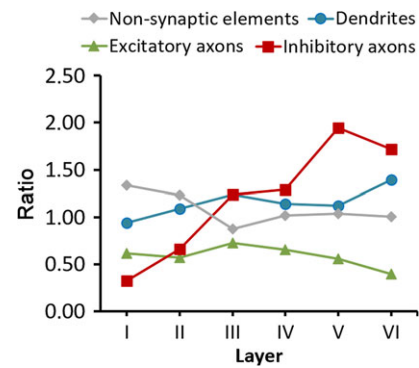


**Figure 9.** Ratios between the proportion of mitochondria located in different subcellular compartments, and the proportions of these compartments in the neuropil. Ratios have been calculated for the 6 cortical layers from data shown in Tables 2 and 3. A value of 1.00 would indicate that the proportion of mitochondria located in this compartment corresponds to the proportion of this compartment in the neuropil. Values over or under 1.00 indicate that mitochondria are relatively more or less abundant in that compartment, respectively.

estimation of the volume fraction of mitochondria at several locations within each stack, so sampling errors are minimized. Since these stacks of images can be visualized and navigated in 3D, the cell processes containing mitochondria can be followed and identified as dendrites, axons, or nonsynaptic elements, based on the presence of synapses. In addition, since synapses have also been identified and classified in these same stacks (Santuy et al. 2018a, 2018b), the possible relationship between mitochondria and synaptic density can also be established.

### Mitochondria in Axons, Dendrites, and Nonsynaptic Elements

Neurons consume most of the energy in the brain, and most of that energy is related to synaptic transmission. Therefore, a higher energetic supply to axon terminals and dendrites would be expected (Overly et al. 1996; Attwell and Laughlin 2001; Harris et al. 2012). Mitochondria are found closely associated with synapses and it has been shown that they can be tethered to vesicle release sites on the presynaptic site (Rowland et al. 2000), where they not only provide ATP but also act as calcium buffers. Synaptic overactivity seems to recruit mitochondria to synapses, whereas prolonged synaptic silence releases mitochondria from these sites. This recruitment occurs through variations in the ADP/ATP ratio and alterations of the attachment of mitochondria by changes in the concentration of  $Ca^{2+}$  (Li et al. 2004; Harris et al. 2012; Obashi and Okabe 2013).

The highest volume fraction of mitochondria was found in layer IV, while the lowest volume fractions were found in layers I and VI. This distribution resembles synapse density, for which the highest density was found in layer IV and the lowest density in layer VI (Anton-Sanchez et al. 2014; Santuy et al. 2018b). However, the distribution of mitochondria most probably depends not only on the presence of synapses, but also on the activity of these synapses. For example, layer IV of the somatosensory cortex receives thalamic afferences that relay information in a very reliable manner, and these fibers have high firing rates to ensure the efficacy of the transmission. To maintain such activity, they require a high density of mitochondria, which are associated with synaptic vesicle pools (Rodriguez-Moreno et al. 2017).



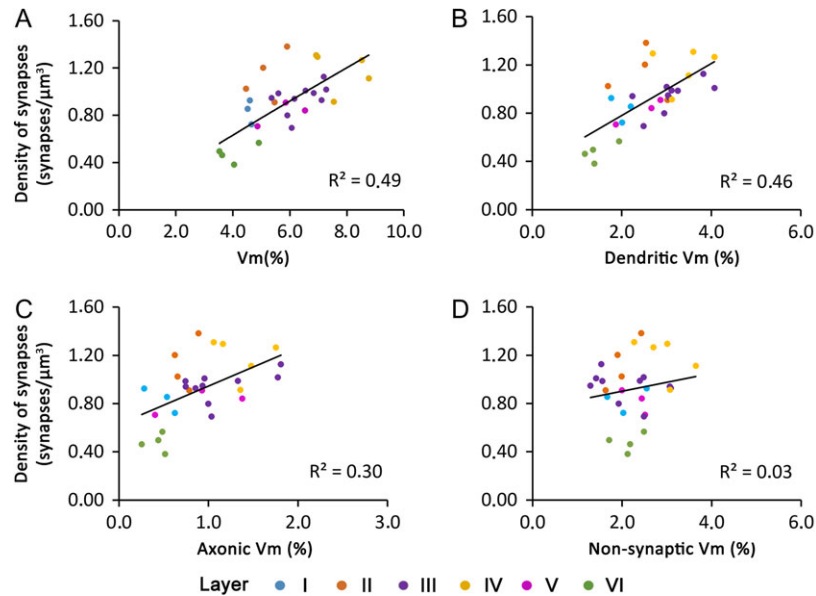


**Figure 10.** Correlation between the density of synapses and the volume fraction of mitochondria located in different subcellular compartments. Correlation between the density of synapses in the neuropil and the volume fraction of mitochondria (Vm) (A), the volume fraction of mitochondria located in dendrites (B), the volume fraction of mitochondria located in axons (C), and the volume fraction of mitochondria located in nonsynaptic elements (D). Data from the 6 cortical layers have been color-coded according to the legend in A.

In the present study, the majority of the mitochondria were found to be located in dendrites, in line with previous reports (Wong-Riley and Carroll 1984; Wong-Riley 1989). In our samples, the ratio between the volumes of dendritic mitochondria to axonic mitochondria is about 75:25, while the ratio between the volume occupied by dendrites and axons is about 60:40. Therefore, we can conclude that mitochondria are more abundant in dendrites than in axons. We have also found that the correlation between mitochondria and synaptic density is stronger for dendritic than for axonic mitochondria. This may be related to what has been described in previous studies regarding energy consumption. Most energy is expended pumping sodium ions out of cells (Attwell and Laughlin 2001); since the postsynaptic side has higher signaling-related sodium influx, the amount of energy required is larger than in the pre-synaptic side (Attwell and Laughlin 2001; Howarth et al. 2012). In inhibitory synapses, the energy consumption at the postsynaptic side is thought to be lower than in excitatory synapses, since the reversing potential of the chloride is closer to the resting potential (Attwell and Laughlin 2001; Howarth et al. 2010, 2012; Harris et al. 2012; Kann et al. 2014).

It is important to note that despite the fact that mitochondria are abundant in dendrites, the presence of these organelles inside dendritic spines is rather rare in the neocortex. Indeed, in a previous 3D electron microscopy study, we found no mitochondria inside any of the more than 4500 dendritic spines analyzed (Santuy et al. 2018b). The present study confirms that result from a different perspective, since here we have specifically targeted the location of mitochondria in different subcellular compartments and, again, we have never found mitochondria inside dendritic spines. This is in line with what has been reported in the somatosensory cortex of the young mouse using 3D reconstructions (Kasthuri et al. 2015). In that study, mitochondria were found inside spines in only 3 out of 1425 cases. Earlier studies have also reported the occasional presence of mitochondria in spines of the visual cortex of the squirrel monkey and macaque (Carroll and Wong-Riley 1984;

Wong-Riley et al. 1989), and in the somatosensory cortex of the cat (Jones and Powell 1969), but we lack quantitative information in these cases. The presence of mitochondria in dendritic spines seems to be more common in the hippocampus than in the neocortex. For example, in CA1 the mean percentage of spines containing mitochondria has been reported to be around 5% (Li et al. 2004). An even higher percentage has been reported in branched dendritic spines of CA3, where 13% of the complete spine heads examined through serial sections contained mitochondria (Chicurel and Harris 1992). This proportion is inverted in granule cells of the olfactory bulb, where 87% of their spines contain mitochondria (Cameron et al. 1991). Therefore, the absence or scarcity of mitochondria within dendritic spines seems to be a unique feature of the neocortex and suggests that the relationship between mitochondria and synapses is regulated by different mechanisms in different regions of the brain. The reasons and implications of this heterogeneous distribution of mitochondria in spines remain unknown and need further research.

In the presynaptic side, mitochondria provide energy to the synaptic release machinery and to different kinds of transporters, and they also participate in the synthesis of neurotransmitters and the buffering of  $\text{Ca}^{2+}$  (Brodin et al. 1999). We found that mitochondria were more common in excitatory axons than in inhibitory axons, with a ratio of about 80:20. In this case, the ratio between the volume occupied by excitatory versus inhibitory axons is about 85:15, so inhibitory axons are richer in mitochondria than excitatory axons. This may be related to studies that point to a higher metabolic cost of inhibitory neurons versus excitatory neurons (Wong-Riley and Carroll 1984; Wong-Riley 1989; McCasland and Hibbard 1997; Howarth et al. 2012). Inhibitory neurons are also functionally heterogeneous (Ascoli et al. 2008; Markram et al. 2015; Kubota et al. 2016; Tremblay et al. 2016; Feldmeyer et al. 2018), so their energy consumption would also depend on their electrical activity (Kann et al. 2014). We also found that the proportion of mitochondria located in inhibitory axons tends to increase

towards infragranular layers, while the volume fraction of inhibitory axons and the density of inhibitory synapses decrease (Santuy et al. 2018b). This could be related to the morphological and functional heterogeneity of inhibitory cells in the cortex, as commented above. For example, basket cells, which are fast spiking interneurons, are particularly abundant in layer VI in the hindlimb representation of the somatosensory cortex of P14 rat and other inhibitory cell types also show a heterogeneous distribution across layers (Markram et al. 2015).

Myelinated axons were scarce in our samples, and they were only present in layers IV–VI, probably because the animals are not completely mature at this age (Jacobson 1963; Salami et al. 2003). The volume fraction of mitochondria located in myelinated axons was correspondingly low, and even undetectable in layer IV. It is well established that the vast majority of myelinated axons in the cerebral cortex—particularly in layers IV–VI—originate from excitatory neurons (mostly pyramidal cells and thalamocortical neurons). However, some GABAergic interneurons, especially basket cells (Somogyi et al. 1983; DeFelipe et al. 1986; Micheva et al. 2016) have a myelinated axon. In the series of electron micrographs, we could not establish whether these myelinated axons established AS or SS and, therefore, we could not determine whether they were excitatory or inhibitory axons.

Finally, about 41% of the total volume of mitochondria corresponds to nonsynaptic elements—a percentage that is similar to the volume of the neuropil occupied by nonsynaptic elements (39%). We cannot rule out the possibility that some of the cell processes that we have included in this category may be axonic and dendritic segments that do not establish synapses within the stacks analyzed. Therefore, the volume fraction of nonsynaptic elements should be considered as an upper limit, since some of these processes may in fact establish synapses outside the tissue volume studied. Although this uncertainty may affect the absolute values of axons, dendrites, and nonsynaptic elements that we have estimated, it would minimally affect the relative ratio between axons and dendrites, and their corresponding mitochondria, that have been unambiguously identified.

Our present data show that the volume fraction of mitochondria in nonsynaptic elements is not correlated with synaptic density, unlike dendritic and axonic mitochondria. This could be due to the fact that many nonsynaptic elements are probably glial processes. If this were the case, then our results would indicate that there is no correlation between the density of synapses and the presence of mitochondria within glial processes. However, astrocytes are indirectly related to synaptic activity since they participate in the regulation of cerebral blood flow in response to changes in neural activity, and may also provide lactate for the use of neurons, among many other functions (Jackson and Robinson 2017; Nortley and Attwell 2017). Indeed, other studies have reported that mitochondria localize in astrocytic processes near synapses in response to neural activity in cultured hippocampal slices (Jackson et al. 2014; Stephen et al. 2015). This apparent discrepancy can be explained by differences in mitochondrial mobility between astrocytes and neurons. In fact, the mobility of mitochondria in astrocytic processes is less pronounced than in dendrites, it is also lower in vivo than in vitro and varies between brain regions (reviewed in Jackson and Robinson (2017)), so there would be only a subtle accumulation of mitochondria in certain astrocytic processes that would go unnoticed with our methods.

## Concluding Remarks

In this work, we have estimated the volume fraction of neuropil, cell bodies, and blood vessels in the 6 layers of the somatosensory cortex of the young rat with the aim of providing detailed microanatomical data which would lead to a better understanding of neocortical structure in mammals. This set of data will also be useful for the building and refining of realistic models of the cortex that require quantitative information about the relationship between the different tissue components (Markram et al. 2015). We have estimated the percentage of tissue occupied by mitochondria in the neuropil of different cortical layers and within different tissue compartments such as dendrites, axons, and nonsynaptic elements. The presence of mitochondria provides an indirect indicator of energy consumption at different locations. In this respect, we have found a positive relationship between the volume fraction of mitochondria and the density of synapses. In addition, we have found that there are more dendritic mitochondria than axonal mitochondria, not only because the volume of dendrites is larger than the volume of axons, but also because—compared with axons—dendrites are proportionally richer in mitochondria. The mitochondrial content of excitatory axons is homogeneous across layers, while the mitochondrial content of inhibitory axons increases from superficial to deep layers.

## Supplementary Material

Supplementary material is available at *Cerebral Cortex* online.

## Funding

Grants from the following entities: the Spanish Ministerio de Economía y Competitividad (Grants SAF 2015-603-P and the Cajal Blue Brain Project, Spanish partner of the Blue Brain Project initiative from EPFL); the European Union Horizon 2020 research and innovation program under Grant agreement No. 785907 (Human Brain Project, SGA2); and Centro de Investigación en Red sobre Enfermedades Neurodegenerativas (CIBERNED, CB06/05/0066, Spain). Correspondence to: amerchan@fi.upm.es.

## Notes

The authors thank Carmen Alvarez, Miriam Marin and Lorena Valdes for their technical assistance. *Conflict of Interest*: None declared.

## References

- Alonso-Nanclares L, Gonzalez-Soriano J, Rodriguez JR, DeFelipe J. 2008. Gender differences in human cortical synaptic density. *Proc Natl Acad Sci USA*. 105:14615–14619.
- Anderson JC, Kevan ACM, Picanco-Diniz CW. 1992. The neurons in layer 1 of cat visual cortex. *Proc Biol Sci*. 248:27–33.
- Anton-Sanchez L, Bielza C, Merchan-Perez A, Rodriguez JR, DeFelipe J, Larranaga P. 2014. Three-dimensional distribution of cortical synapses: a replicated point pattern-based analysis. *Front Neuroanat*. 8:85.
- Ascoli GA, Alonso-Nanclares L, Anderson SA, Barrionuevo G, Benavides-Piccione R, Burkhalter A, Buzsaki G, Cauli B, Defelipe J, Fairen A, et al. 2008. Petilla terminology: nomenclature of features of GABAergic interneurons of the cerebral cortex. *Nat Rev Neurosci*. 9:557–568.

- Attwell D, Laughlin SB. 2001. An energy budget for signaling in the grey matter of the brain. *J Cereb Blood Flow Metab.* 21: 1133–1145.
- Brocard JB, Rintoul GL, Reynolds IJ. 2003. New perspectives on mitochondrial morphology in cell function. *Mol Biol Cell.* 95: 239–242.
- Brodin L, Bakeeva L, Shupliakov O. 1999. Presynaptic mitochondria and the temporal pattern of neurotransmitter release. *Philos Trans R Soc Lond B Biol Sci.* 354:365–372.
- Broskey NT, Daraspe J, Humbel BM, Amati F. 2013. Skeletal muscle mitochondrial and lipid droplet content assessed with standardized grid sizes for stereology. *J Appl Physiol.* 115:765–770.
- Cai Q, Sheng Z-H. 2009. Mitochondrial transport and docking in axons. *Exp Neurol.* 218:257–267.
- Cameron HA, Kaliszewski CK, Greer CA. 1991. Organization of mitochondria in olfactory bulb granule cell dendritic spines. *Synapse.* 8:107–118.
- Carroll EW, Wong-Riley MTT. 1984. Quantitative light and electron microscopic analysis of cytochrome oxidase-rich zones in the striate cortex of the squirrel monkey. *J Comp Neurol.* 222:1–17.
- Chang DT, Honick AS, Reynolds IJ. 2006. Mitochondrial trafficking to synapses in cultured primary cortical neurons. *J Neurosci.* 26:7035–7045.
- Chen H, Chan DC. 2005. Emerging functions of mammalian mitochondrial fusion and fission. *Hum Mol Genet.* 14 Spec No. 2:R283–R289.
- Chicurel ME, Harris KM. 1992. Three-dimensional analysis of the structure and composition of CA3 branched dendritic spines and their synaptic relationships with mossy fiber boutons in the rat hippocampus. *J Comp Neurol.* 325: 169–182.
- Colonnier M. 1968. Synaptic patterns on different cell types in the different laminae of the cat visual cortex. An electron microscope study. *Brain Res.* 9:268–287.
- DeFelipe J, Fairen A. 1993. A simple and reliable method for correlative light and electron microscopic studies. *J Histochem Cytochem.* 41:769–772.
- DeFelipe J, Hendry SH, Jones EG. 1986. A correlative electron microscopic study of basket cells and large GABAergic neurons in the monkey sensory-motor cortex. *Neuroscience.* 17: 991–1009.
- Devine MJ, Kittler JT. 2018. Mitochondria at the neuronal presynapse in health and disease. *Nat Rev Neurosci.* 19:63.
- Dubinsky JM. 2009. Heterogeneity of nervous system mitochondria: location, location, location! *Exp Neurol.* 218:293–307.
- Feldmeyer D, Qi G, Emmenegger V, Staiger JF. 2018. Inhibitory interneurons and their circuit motifs in the many layers of the barrel cortex. *Neuroscience.* 368:132–151.
- García-Cabezas MÁ, John YJ, Barbas H, Zikopoulos B. 2016. Distinction of neurons, glia and endothelial cells in the cerebral cortex: an algorithm based on cytological features. *Front Neuroanat.* 10:107.
- Gray EG. 1959. Axo-somatic and axo-dendritic synapses of the cerebral cortex: an electron microscope study. *J Anat.* 93: 420–433.
- Gundersen HJ, Bagger P, Bendtsen TF, Evans SM, Korbo L, Marcussen N, Moller A, Nielsen K, Nyengaard JR, Pakkenberg B, et al. 1988. The new stereological tools: disector, fractionator, nucleator and point sampled intercepts and their use in pathological research and diagnosis. *APMIS.* 96:857–881.
- Harris JJ, Jolivet R, Attwell D. 2012. Synaptic energy use and supply. *Neuron.* 75:762–777.
- Houser CR, Vaughn JE, Hendry SH, Jones EG, Peters A. 1984. GABA neurons in cerebral cortex. Functional properties of cortical cells. In: Peters A, Jones EG, editors. *Cerebral Cortex.* New York: Plenum Press. p. 63–89.
- Howard V, Reed MG. 2005. *Unbiased stereology: three-dimensional measurement in microscopy.* Oxon, UK: Garland Science/BIOS Scientific Publishers.
- Howarth C, Gleeson P, Attwell D. 2012. Updated energy budgets for neural computation in the neocortex and cerebellum. *J Cereb Blood Flow Metab.* 32:1222–1232.
- Howarth C, Peppiatt-Wildman CM, Attwell D. 2010. The energy use associated with neural computation in the cerebellum. *J Cereb Blood Flow Metab.* 30:403–414.
- Jackson JG, O'Donnell JC, Takano H, Coulter DA, Robinson MB. 2014. Neuronal activity and glutamate uptake decrease mitochondrial mobility in astrocytes and position mitochondria near glutamate transporters. *J Neurosci.* 34: 1613–1624.
- Jackson JG, Robinson MB. 2017. Regulation of mitochondrial dynamics in astrocytes: mechanisms, consequences, and unknowns. *Glia.* 66:1213–1234.
- Jacobson S. 1963. Sequence of myelination in the brain of the albino rat. A. Cerebral cortex, thalamus and related structures. *J Comp Neurol.* 121:5–29.
- Jones EG, Powell TPS. 1969. Morphological variations in the dendritic spines of the neocortex. *J Cell Sci.* 5:509–529.
- Kann O, Papageorgiou IE, Draguhn A. 2014. Highly energized inhibitory interneurons are a central element for information processing in cortical networks. *J Cereb Blood Flow Metab.* 34:1270–1282.
- Kasthuri N, Hayworth KJ, Berger DR, Schalek RL, Conchello JA, Knowles-Barley S, Lee D, Vazquez-Reina A, Kaynig V, Jones TR, et al. 2015. Saturated reconstruction of a volume of neocortex. *Cell.* 162:648–661.
- Kubota Y, Karube F, Nomura M, Kawaguchi Y. 2016. The diversity of cortical inhibitory synapses. *Front Neural Circuits.* 10:27.
- Li Z, Okamoto K, Hayashi Y, Sheng M. 2004. The importance of dendritic mitochondria in the morphogenesis and plasticity of spines and synapses. *Cell.* 119:873–887.
- MacAskill AF, Atkin TA, Kittler JT. 2010. Mitochondrial trafficking and the provision of energy and calcium buffering at excitatory synapses. *Eur J Neurosci.* 32:231–240.
- MacAskill AF, Kittler JT. 2010. Control of mitochondrial transport and localization in neurons. *Trends Cell Biol.* 20: 102–112.
- Markram H, Muller E, Ramaswamy S, Reimann MW, Abdellah M, Sanchez CA, Ailamaki A, Alonso-Nanclares L, Antille N, Arsever S, et al. 2015. Reconstruction and simulation of neocortical microcircuitry. *Cell.* 163:456–492.
- McCasland JS, Hibbard LS. 1997. GABAergic neurons in barrel cortex show strong, whisker-dependent metabolic activation during normal behavior. *J Neurosci.* 17:5509–5527.
- Merchán-Pérez A, Rodríguez JR, Alonso-Nanclares L, Schertel A, DeFelipe J. 2009. Counting synapses using FIB/SEM microscopy: a true revolution for ultrastructural volume reconstruction. *Front Neuroanat.* 3:14.
- Merchán-Pérez A, Rodríguez JR, Gonzalez S, Robles V, Defelipe J, Larranaga P, Bielza C. 2014. Three-dimensional spatial distribution of synapses in the neocortex: a dual-beam electron microscopy study. *Cereb Cortex.* 24: 1579–1588.
- Micheva KD, Wolman D, Mensh BD, Pax E, Buchanan J, Smith SJ, Bock DD. 2016. A large fraction of neocortical myelin

- ensheathes axons of local inhibitory neurons. *Elife*. 5: e15784.
- Mironov A. 2017. Stereological morphometric grids for ImageJ. *Ultrastruct Pathol*. 41:126.
- Morales J, Alonso-Nanclares L, Rodriguez J-R, Defelipe J, Rodriguez A, Merchan-Perez A. 2011. Espina: a tool for the automated segmentation and counting of synapses in large stacks of electron microscopy images. *Front Neuroanat*. 5:18.
- Muralidhar S, Wang Y, Markram H. 2014. Synaptic and cellular organization of layer 1 of the developing rat somatosensory cortex. *Front Neuroanat*. 7:52.
- Nortley R, Attwell D. 2017. Control of brain energy supply by astrocytes. *Curr Opin Neurobiol*. 47:80–85.
- Obashi K, Okabe S. 2013. Regulation of mitochondrial dynamics and distribution by synapse position and neuronal activity in the axon. *Eur J Neurosci*. 38:2350–2363.
- Overly CC, Rieff HI, Hollenbeck PJ. 1996. Organelle motility and metabolism in axons vs dendrites of cultured hippocampal neurons. *J Cell Sci*. 109:971–980.
- Paxinos G, Watson C. 2007. *The Rat Brain in Stereotaxic Coordinates*. 6th ed. London: Academic Press.
- Peters A, Palay SL. 1996. *The morphology of synapses*. *J Neurocytol*. 25:687–700.
- Peters A, Palay SL, Webster H deF. 1991. *The fine structure of the nervous system. Neurons and their supporting cells*. 3rd ed. New York: Oxford University Press.
- Revishchin AV, Garey LJ. 1996. Mitochondrial distribution in visual and auditory cerebral cortex of the harbour porpoise. *Brain Behav Evol*. 47:257–266.
- Rizzuto R, De Stefani D, Raffaello A, Mammucari C. 2012. Mitochondria as sensors and regulators of calcium signaling. *Nat Rev Mol Cell Biol*. 13:566–578.
- Roberts RC, Barksdale KA, Roche JK, Lahti AC. 2015. Decreased synaptic and mitochondrial density in the postmortem anterior cingulate cortex in schizophrenia. *Schizophr Res*. 168:543–553.
- Roberts RC, Roche JK, Conley RR. 2008. Differential synaptic changes in the striatum of subjects with undifferentiated versus paranoid schizophrenia. *Synapse*. 62:616–627.
- Rodriguez-Moreno J, Rollenhagen A, Arlandis J, Santuy A, Merchan-Pérez A, DeFelipe J, Lübke JH, Clasca F. 2017. Quantitative 3D ultrastructure of thalamocortical synapses from the “lemniscal” ventral posteromedial nucleus in mouse barrel cortex. *Cereb Cortex*. doi:10.1093/cercor/bhx187.
- Rowland KC, Irby NK, Spirou GA. 2000. Specialized synapse-associated structures within the calyx of held. *J Neurosci*. 20:9135–9144.
- Sakata JT, Jones TA. 2003. Synaptic mitochondrial changes in the motor cortex following unilateral cortical lesions and motor skills training in adult male rats. *Neurosci Lett*. 337: 159–162.
- Salami M, Itami C, Tsumoto T, Kimura F. 2003. Change of conduction velocity by regional myelination yields constant latency irrespective of distance between thalamus and cortex. *Proc Natl Acad Sci USA*. 100:6174–6179.
- Santuy A, Rodríguez JR, DeFelipe J, Merchán-Pérez A. 2018a. Study of the size and shape of synapses in the juvenile rat somatosensory cortex with 3D electron microscopy. *eNeuro*. 5:ENEURO.0377-17.2017.
- Santuy A, Rodríguez JR, DeFelipe J, Merchán-Pérez A. 2018b. Volume electron microscopy of the distribution of synapses in the neuropil of the juvenile rat somatosensory cortex. *Brain Struct Funct*. 223:77–90.
- Schwarz TL. 2013. Mitochondrial trafficking in neurons. *Cold Spring Harb Perspect Biol*. 5:a011304.
- Shaw JM, Nunnari J. 2002. Mitochondrial dynamics and division in budding yeast. *Trends Cell Biol*. 12:178–184.
- Somogyi P, Kisvarday ZF, Martin KA, Whitteridge D. 1983. Synaptic connections of morphologically identified and physiologically characterized large basket cells in the striate cortex of cat. *Neuroscience*. 10:261–294.
- Stephen T-L, Higgs NF, Sheehan DF, Al Awabdh S, López-Doménech G, Arancibia-Carcamo IL, Kittler JT. 2015. Miro1 regulates activity-driven positioning of mitochondria within astrocytic processes apposed to synapses to regulate intracellular calcium signaling. *J Neurosci*. 35: 15996–16011.
- Sumpter PQ, Mann DM, Davies CA, Yates PO, Snowden JS, Neary D. 1986. An ultrastructural analysis of the effects of accumulation of neurofibrillary tangle in pyramidal neurons of the cerebral cortex in Alzheimer’s disease. *Neuropathol Appl Neurobiol*. 12:305–319.
- Takahara Y, Inatani M, Eto K, Inoue T, Kreymerman A, Miyake S, Ueno S, Nagaya M, Nakanishi A, Iwao K, et al. 2015. In vivo imaging of axonal transport of mitochondria in the diseased and aged mammalian CNS. *Proc Natl Acad Sci USA*. 112:10515–10520.
- Tang Y, Nyengaard JR, Pakkenberg B, Gundersen HJ. 1997. Age-induced white matter changes in the human brain: a stereological investigation. *Neurobiol Aging*. 18:609–615.
- Tao M, You CP, Zhao RR, Liu SJ, Zhang ZH, Zhang C, Liu Y. 2014. Animal mitochondria: evolution, function, and disease. *Curr Mol Med*. 14:115–124.
- Todorova V, Blokland A. 2017. Mitochondria and synaptic plasticity in the mature and aging nervous system. *Curr Neuropharmacol*. 15:166–173.
- Tremblay R, Lee S, Rudy B. 2016. GABAergic interneurons in the neocortex: from cellular properties to circuits. *Neuron*. 91: 260–292.
- Wong-Riley MT. 1989. Cytochrome oxidase: an endogenous metabolic marker for neuronal activity. *Trends Neurosci*. 12: 94–101.
- Wong-Riley MT, Carroll EW. 1984. Quantitative light and electron microscopic analysis of cytochrome oxidase-rich zones in V II prestriate cortex of the squirrel monkey. *J Comp Neurol*. 222:18–37.
- Wong-Riley MT, Trusk TC, Tripathi SC, Hoppe DA. 1989. Effect of retinal impulse blockage on cytochrome oxidase-rich zones in the macaque striate cortex: II. Quantitative electron-microscopic (EM) analysis of neuropil. *Vis Neurosci*. 2:499–514.